BARC
NEWSLETTER

Celebrating the spirit of Diamond Jubilee Year
Department of Atomic Energy Tableau in the 66th Republic Day Parade 2015 at Rajpath, New Delhi

Atoms in the Service of the Nation

Celebrating its diamond jubilee year, the Department of Atomic Energy portrays in its tableau, its expertise in harnessing the tremendous potential of the atom for societal benefits in the service of the nation. The tableau is led by a white dove atop an atomic orbital symbolising the conviction of the nation to spread the message - 'Atoms for Peace'. It also pays a somber homage to the visionary Dr. Homi Jehangir Bhabha, founding father of the Indian Nuclear Programme. The trailer portion is conceptually divided into three parts depicting peace, progress and prosperity, vis-a-vis the service deliverables of the Department. The first part symbolises progress in the field of medical technology depicting the indigenously developed 'Bhabhatron' machine, used in radiotherapy and delivering affordable healthcare. The colourful flora, following it, posturizes prosperity in food and agriculture through mutation breeding technology to provide disease resistant and high yielding seeds; food irradiation techniques that increase the shelf life of the produce. Lastly, standing tall, the indigenous Nuclear Reactor showcases the advantage of nuclear energy to provide an unlimited supply of clean and green energy for the sustained progress of the nation.

-**DEPARTMENT OF ATOMIC ENERGY**

CONTENTS

From the Editor's Desk

Welcome to the May-June 2015 issue of the BARC Newsletter. We have featured five articles on different research areas ranging from waste management to water treatment. BARC has proven expertise in the backend of the nuclear fuel cycle. Hull compaction process, one of the waste volume reduction techniques and the development of Hull Drying Unit in BARC are highlighted in the first article. BARC has been developing various water treatment technologies. A manual and rural-friendly water treatment system for producing safe drinking water developed by the Desalination Division is presented in the last article. We once again appeal to the readers to contribute articles to the BARC newsletter.

Dr. G. Ravi Kumar
On behalf of the Editorial Committee

Evaluation of Performance Characteristics of a Hull Drying Unit

C.K. Chakrabarti, K.M. Singh and K. Banerjee
Fast Reactor Waste Management Directorate,
Nuclear Recycle Board
and
S. Bhowmick and K.T. Shenoy
Chemical Engineering Division

Abstract

In the back end of the fuel cycle, hull compaction is an important waste management practice for volume reduction of hull waste. The hull waste should be completely dried of wash solution before high pressure compaction to avoid radiolysis and corrosion phenomena. A Hull Drying Unit was designed, fabricated and installed and the influence of the operating parameters on the performance of this unit was investigated experimentally. This experimental study helped to optimize the design and operating parameters of the hull drying system. The study also shows that direct contact hot air heating is a promising technique for drying of hull waste and can be adopted in the Fast Reactor Fuel Cycle Facility.

Introduction

India adopted the three-stage nuclear power program to secure the country's long term self-sufficiency in the energy sector through the utilization of thorium reserves. Thorium will be introduced in Stage-II in a Fast Breeder Reactor (FBR) as blanket material and transmuted to uranium-233. This uranium-233 will be used in the third stage as fuel along with the abundantly available thorium. Obviously the Fast Reactor Fuel Cycle Facility (FRFCF) will play an important role in India's three-stage nuclear power program. A constant effort is being made in the minimization of waste volume in such nuclear recycle facility. Recently a hull compaction system was conceptualized by the Nuclear Recycle Board (NRB) to reduce the volume of hull waste generated during reprocessing of spent fuel from Pressurized Heavy Water Reactor (PHWR) [1]. This hull compaction process will also be adopted in FRFCF. Prior to compaction, liquid content in the hull waste should be removed completely to avoid radiolysis and corrosion phenomena.

In FRFCF, two types of (Stainless Steel)-D9 hull pieces will be generated from the Fuel Reprocessing Plant (FRP), one from Fuel Sub Assembly (FSA) (of dimension 6.6 mm OD, 0.45 mm wall thicknesses, and 40 mm) length and another from Radial Blanket Sub Assembly (RSA) (of dimension 14.33 mm OD, 0.9 mm wall thickness, and 40 mm length). Heat required for drying of these hull pieces can be supplied by direct contact method or indirect method. According to Ladre et al. [2] indirect heating by means of resistance element or induction coil placed around the drum has been found to be of poor performance. The void spaces among heterogeneously distributed hollow hull pieces will be occupied with air. Consequently the central region of drum will take a lot of time to reach the drying temperature. Conversely, this method of heating is advantageous with respect to minimum secondary off-gas generation. The direct contact heating by hot air or inert gas has been opted for plant scale by reprocessing plants at La Hague, France [3] and Tokai, Japan [4]. At La Hague plant, the operating conditions of dryer were chosen to maintain the hot gas temperature below 200°C and drying time less than 30 minutes per can. At Tokai plant hulls, end pieces and metal wastes in the check capsule are dried in the chamber filled with nitrogen (130 torr) at 140°C. The direct contact heating is quite efficient heating method with lesser time required for drying. But a considerable volume of secondary off-gas is generated in this heating method. The off-gas needs to be treated in an off-gas treatment system.

In the present work, experimental investigation has been carried out to evaluate the performance of a Hull Drying Unit (HDU) and optimize the process and design parameters. The direct contact hot air drying was adopted as SS hull is not pyrophoric in nature. SS tube pieces having dimensions similar to FSA hull was used in the experiments. The hot air flow rate will be kept as low as possible to prevent the carryover/ entrainment of any active particles from the hull pieces. The low air flow rate will also minimize the off-gas load. A lower temperature shall be selected for drying air to minimize the power consumption in

the drying operation and minimizing the heat load in the off gas treatment process. Hence, the main objectives of the present study were to identify the effect of hot air flow rate and air temperature on drying time and optimize the process parameters.

Experimental Details

Experimental Setup

A simplified diagram of the experimental setup is presented in Figure 1. The hull drying unit consists of two concentric cylinders made of mild steel. The internal diameters of these cylinders are 360 mm (inner) and 470 mm (outer) respectively. The thickness of both cylinders is 5 mm. The annulus space between these two cylinders is filled with glass wool insulation to minimize heat loss. The height of the drying unit without top lid is 1200 mm. 40 NB, Sch–40 size pipes are used for hot air entry and off-gas exit nozzle. A horizontal annular disc support having 270 mm opening diameter is fitted inside the inner cylinder at an elevation of 250 mm from the base. The top cover is connected to the drying unit by a hinge joint. The cover was also insulated with glass wool insulation. During the experiment, the hull batching can is placed on the disc support. The hull batching can is fitted with a perforated plate at the bottom for the entry of hot air. The internal diameter and height of the can is 326 mm and 700 mm, respectively. A handle is

BV: Ball valve
GV: Globe valve
H/ T: Humidity transmitter
PG: Pressure gauge
PLR: Paperless recorder
PRV: Pressure regulating valve
RM: Rotameter
T/ C: Thermocouple

SS tube cut pieces used as simulated hull pieces

Hull Drying Unit
1. Hot air inlet
2. Horizontal disc support
3. Hull batching can
4. Glass wool insulation
5. Outer cylinder
6. Inner cylinder
7. Hinge
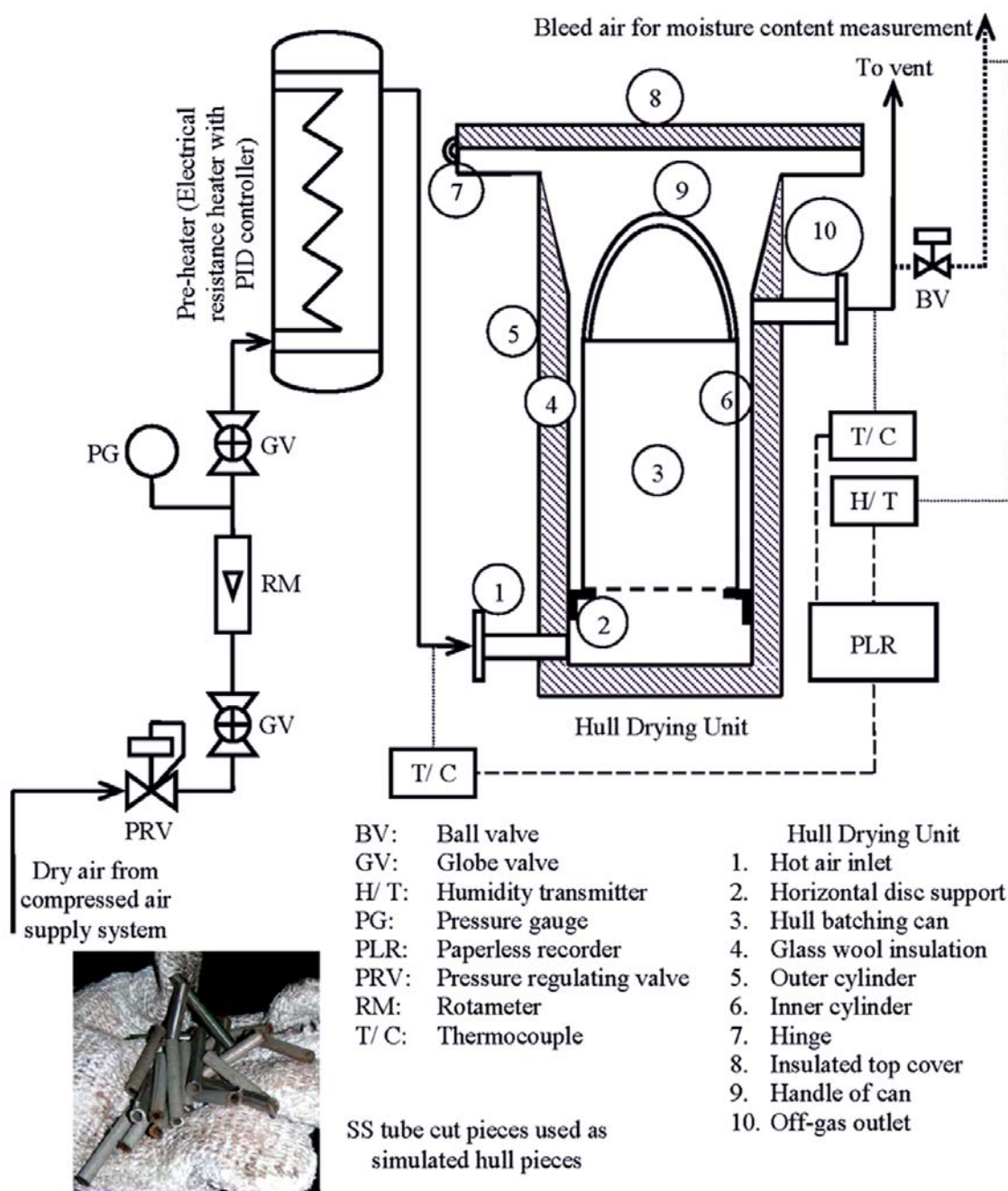8. Insulated top cover
9. Handle of can
10. Off-gas outlet

Fig 1: Schematic sketch of experimental setup

provided with the can for lifting and shifting of the Can. SS tube pieces with an average length of 40 mm were used as simulated hull pieces. The outer diameter and thickness of SS tube are 6.6 mm and 1 mm respectively.

The compressed air supply system consists of a screw compressor and a pressure swing adsorption type air drying unit. The volumetric flow rate (SLPM) of dry air was metered by a rotameter. Then the air was passed through a series of four pre-heaters to obtain desired air temperature. The air temperature at the outlet of the pre-heater was maintained by a PID controller. The air temperature at the inlet and exit of the hull drying unit was measured by K type thermocouples. The exhaust gas was discharged to the atmosphere at a certain height from the ground level. A small portion of exit gas was sent as bleed through a ½" SS tube line. The moisture content in the bleed air was measured using a dew point transmitter. All the measured data was stored in a paperless recorder.

Experimental Procedures

SS tube pieces weighing 21.02 kg were taken into the hull batching can. A Stainless Steel drum filled with raw water was used as an immersion tank for hulls. The hull batching can containing SS tube pieces was lifted by an electrical hoist and immersed in the water of the immersion tank. A small quantity of air was passed through the water to assist permeation of water to all void spaces in the randomly packed bed of hull pieces. After 30 minutes, the can was lifted over the water level and kept in hanging position for drip drying. Sufficient time (4 hours) was provided for completion of drip drying. The weight of the hull batching can with tube pieces was weighed in an electronic weight machine before and after water immersion and dripping process. The amount of water remained inside the SS tube pieces was determined from the weight difference. The air flow through the drying unit was started. The pre-heaters were switched on. After obtaining a stable air temperature at the inlet of drying unit, the air flow was stopped momentarily. The top lid of dryer was opened. The hull batching can carrying wet SS tubes was charged inside the dryer. The top cover was closed and made leak-tight using C clamps. The hot air flow was started again.

The initial moisture content of the dry air was noted before charging the wet hull pieces. After complete drying, the moisture content of the bleed air will be equal to the initial value and the actual drying time was found out from this indication. Also at the end

of each experiment, the hull pieces were immediately withdrawn from the dryer. They were then thoroughly inspected for traces of water visually as well as by weighing. It was confirmed that the moisture content of the bleed air is a precise indication of complete drying. A pictorial representation of the experimental procedures is shown in Figure 2.
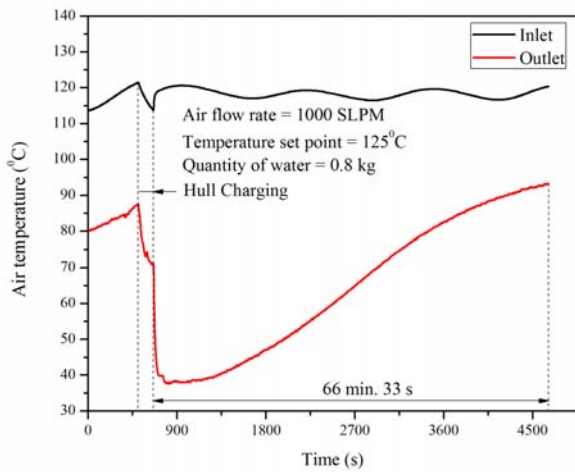

Fig. 2: Experimental stages – (a) immersion of hull pieces in the water, (b) air sparging, (c) water dripping, (d) weighing, (e) loading of hull batching can inside dryer, and (f) closing of lid with C clamps.
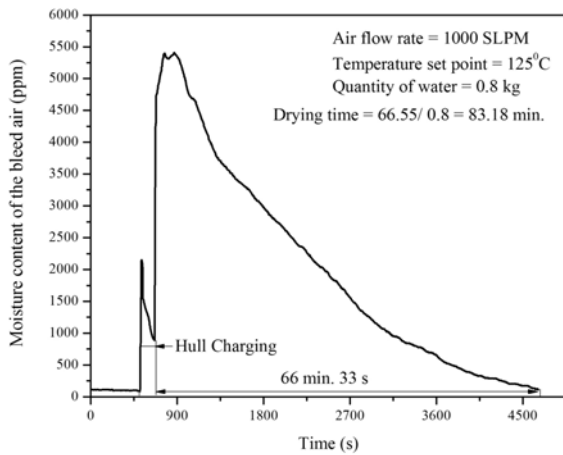
Results and Discussion

In the present study, the volumetric flow rate of air was varied in the range of 720 – 2000 SLPM. The inlet air temperature was from 115 – 135°C. Figure 3 shows the plot of inlet and outlet temperatures of air versus time for specific conditions. Corresponding time variation in moisture content of the bleed air is presented in Figure 4. Parametric studies have been conducted to assess the influence of operating parameters on the performance of the hull dryer.
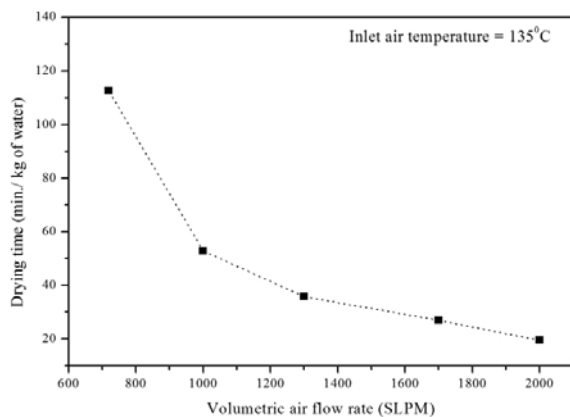
Effect of Volumetric Air Flow Rate

The effect of volumetric air flow rate on drying time is shown in Figure 5. It was observed that the time required for complete drying of hull pieces decreases

Fig. 3: Air temperature at inlet and outlet of hull dryer as a function of time

Fig. 4: Time variation of moisture content in the bleed air
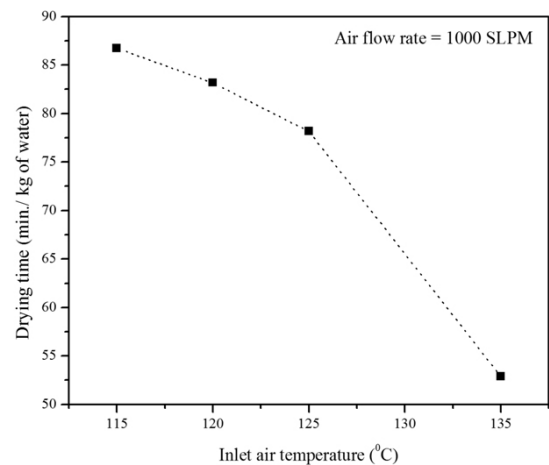

Fig. 5: Influence of volumetric air flow rate on drying time

with increase in volumetric air flow rate. This is on account of the enhanced heat and mass transfer. The quantity of water trapped inside hull pieces was different in each experiment. The range of variation was in the order of 0.65 – 1.02 kg. The measured drying times were normalized through dividing by quantity of water. As per requirement, the drying time shall be lesser than 90 minutes/ kg of water. A higher volumetric flow rate may increase the off gas load. Considering the abovementioned constraints the air flow rate of 1000 SLPM was selected. Now the inlet air temperature can be optimized to minimize the heater power requirement.

Effect of Inlet Air Temperature

Figure 6 shows the influence of inlet air temperature on drying time. It was noted that the drying time increases with decrease in inlet air temperature. The drying time corresponding to air temperature of 115^0C was 86.73 min./ kg of water. Hence, further decrease in inlet air temperature will cross our requirement, i.e., 90 minutes/ kg of water.

Fig. 6: Effect of inlet air temperature on drying time

Future Plant Scale Design Consideration

Multiple numbers (3-4) of such drying units can be planned inside the hot cell for drying the hull pieces placed inside the hull batching can. Individual hot air line connection shall be provided for every drying unit. The off gas from individual unit will be connected to the common off gas header which will be passed through off gas condenser, packed scrubber, chiller, demister, heater and two stages of HEPA filters before releasing through the stack. The secondary waste will be monitored and accordingly treated either through vitrification route or low level waste treatment route. Hot air generator with its sub header shall be placed

in the adjacent service distribution gallery for supplying hot air to those drying unit placed inside the hot cell. Top lid of drying unit can be opened and closed remotely by Master Slave Manipulator (MSM) and incell crane. The batching-can loading and unloading can be also done by the incell crane. A modified batching can design has also been planned so that liquid dripping can be avoided and the remote handling operation can be simplified.

Conclusion

The direct contact heating by hot air can be considered as a possible option for removal of liquid from SS hull pieces which will be generated in FRFCF. The influence of operating parameters on the performance of a HDU was investigated experimentally. It was found that the drying time decreases with increase in air flow rate and air temperature. From the analysis of experimental results, the optimum air flow rate and temperature were found to be 1000 SLPM (64.4 Nm^3/h.), and 115^{0}C respectively. However, the quantity of hull pieces to be placed inside the hull batching can in FRFCF is still under review. In a real case scenario the quantity of hull pieces will be different from the quantity used in the experiments. In future, the hull drying experimental setup will be used to estimate the drying time per hull batching can after fixing the quantity of hull pieces to be placed inside one can in the FRFCF.

References

1. A. A. Manole, P. P. Karkhanis, K. Agarwal, S. Basu, "*Development of Hull Compaction System for Nuclear Recycle Facility*", BARC Newsletter, Issue No. 334, 32 – 37, Sept.- Oct. 2013.

2. M. Ladre, S. Le Cocq, G. Limeuil, "*Method of Drying Metallic Waste of Pyrophoric Tendencies that is to be Compacted; Apparatus and Compacting Canister Associated with Said Method*", Patent No: US 6,880,265 B2, April 19, 2005.

3. F.Chotin, Ph. Pinson, "*The Atelier De Compactage Des Coques (ACC) Facility: The R&D Programme*", IAEA-SM-357/30.

4. Hiroshi Kojima, Kouichiro Kurakata, "*Safety Evaluation for Hull Waste Treatment Process in JNC*", WM'02 Conference, February 24-28, 2002, Tucson, AZ.

Molecular Modelling Guided Experimental Study for Isotopic Enrichment of Gadolinium

A. Boda, S.K. Arora, A.K. Singha Deb, J.M. Joshi, M. Jha, S. Govalkar, P.V. Kadale, Sk. M. Ali, S. Mukhopadhyay and K.T. Shenoy
Chemical Engineering Division

Abstract

Molecular modelling and experimental studies were performed to predict the feasibility of Gd isotope separation using crown ether grafted resin. BP and B3LYP functional - based DFT calculations foretell the complexation stability order of Gd^{3+} ion as DCH18C6>B15C5>DB18C6 as observed in the experiment. The calculated isotopic separation factor shows that DB18C6 is the promising candidate. Hence, CMPS grafted DB18C6 resin was chosen for the isotope separation of Gd. The adsorption capacity of the resin for Gd^{3+} ion was found to be 1mg/g. The separation coefficients ($\varepsilon \times 10^3$) were found to be 6.3, 3.4, 9.7 and 11.1 for the isotopic pair of 155/158, 157/158, 155/160 and 157/160 respectively and shows promise for future study.

Introduction

Naturally occurring gadolinium (Gd) consists of 7 stable isotopes. ^{152}Gd, ^{154}Gd, ^{155}Gd, ^{156}Gd, ^{157}Gd, ^{158}Gd and ^{160}Gd of which abundance ratios are 0.20, 2.18, 14.80, 20.47, 15.65, 24.84 and 21.86 at%, respectively [1]. Gadolinium has the highest cross section for the capture of thermal neutrons compared to other elements. Further, ^{157}Gd and ^{155}Gd have the higher cross sections of 254000 and 60900 barns respectively compared to the remaining isotopes of Gd. Natural Gd is currently used as a burnable poison in nuclear fuel but the use of only Gd-155/157 has been proposed as this would create an even more effective burnable poison [2].

The three main methods for the production of stable isotopes are: distillation [3], centrifuge [4] and electromagnetic separation [5, 6] (calutron), but each of these methods has its own limitations. The chemical exchange isotope separations, on the other hand, have usually small separation coefficients and necessitate a longer time duration to obtain enriched products; however chemical exchange isotope separations are inherently equilibrium processes and are therefore considered as energy conservation processes. Separation of isotopes by chromatography is one of the most effective chemical exchange methods, which is based on the chemical equilibrium between isotopic species distributed between the stationary phase and mobile solution phase. It has been applied successfully to the separation of isotopes of various elements of lower mass [7-14].

Because crown ethers are good complex forming compounds for most of the metal ions, isotope separations are obviously best investigated by means of chemical reactions with crown ethers [15-17]. The separation of isotopes using dibenzo- and dicyclohexyl-18-crown-6 [18] was first demonstrated by Jepson et al. [18]. Because of high isotopic separation factors with crown ethers, they are recently being used as promising isotope enrichment agents [19].

The application of molecular modelling is growing rapidly with continuing developments in computer power, robust algorithms, and availability of software. Today molecular modelling can sometimes provide useful estimates of the properties and behavior of materials, even before they have been synthesized and it also provides useful estimates of the parameters needed for traditional chemical engineering process development & design. Development of suitable adsorbents for the separation of isotopes by means of experiment alone is a difficult task which can be made little easier by predicting the enrichment factor for the elements of interest employing molecular modelling [20-24]. The present work reports the molecular modelling and experimental study to predict the feasibility of Gd isotope separation using Chloromethylated polystyrene (CMPS) grafted DB18C6 crown ether resin.

Molecular modelling

Isotope effect is a quantum mechanical phenomenon and hence it is obvious to study the isotope effect of

gadolinium using quantum computation-based molecular modelling.
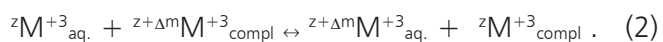
Computational protocol

All the geometries of the free as well as complexes are optimized using Turbomole[25] package at BP86/SV(P) level of theory[26]. Single point energy calculations were carried out on optimized complexes at B3LYP/TZVP [27, 28] level. The optimized structures of different chemical species are drawn using MOLDEN molecular visualization graphics programme. The binding energies (ΔE) are calculated for the complexation of metal ions (M) with ligands (L): M + L = ML as given below,

$$\Delta E = E_{ML} - (E_M + E_L) \qquad (1)$$

Here E_{ML}, E_M and E_L are the energies of the molecular complex, metal ion and ligand respectively. The selectivity of the crown ether is demonstrated by the calculated values of ΔE of Gd^{3+} ion with the ligands.

Theory

Isotope effects in chemical exchange reactions are mainly quantum mechanical and hence cannot be explained by classical statistical mechanics. Quantum electronic structure theory based computational methods are becoming increasingly central to understanding the fractionation of stable isotopes in various chemical exchange systems. The equilibrium constants for isotopic exchange reactions from spectroscopic data was reported by Urey et al.[29]. The separation factor for the following isotopic exchange reaction

$$^{z}M^{+3}{}_{aq.} + {}^{z+\Delta m}M^{+3}{}_{compl} \leftrightarrow {}^{z+\Delta m}M^{+3}{}_{aq.} + {}^{z}M^{+3}{}_{compl} . \qquad (2)$$

z = atomic mass and M^{+3}= metal ion. (compl means complexed by the ligand) can be written in terms of reduced partition function ratio (RPFR, f^r) as [30]

$$\alpha = f^r M^{+3}{}_{aq.} / f^r M^{+3}{}_{compl} \qquad (3)$$

f^r is given by

$$f^r = Z_{vib}{}^{z+\Delta m}M^{+3}\Pi_i(h\nu_i{}^{z+\Delta m}M^{+3}/k_BT)/Z_{vib}{}^{z}M^{+3}\Pi_i(h\nu_i{}^{z}M^{+3}/k_BT) \qquad (4)$$

Here, Z and n are the vibrational partition function and frequency, k_B and h are the Boltzmann and Planck constants respectively and T is the temperature. The main input required for the evaluation of RPFR and separation factor is the harmonic vibrational frequency of the system of interest.
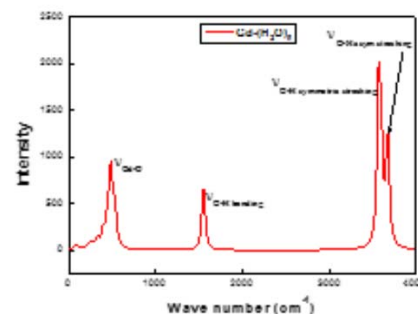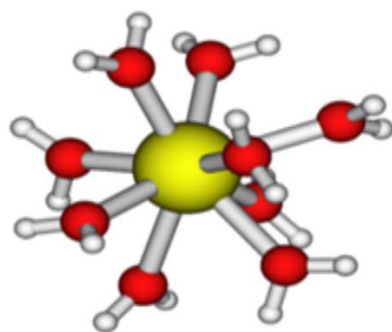

Fig. 1: Optimized geometry of hydrated Gd^{3+} ion and calculated IR spectra

Results and Discussion

Molecular Modelling

Most of the isotopic enrichment of the elements takes place from aqueous feed solution. Therefore, it is of primary importance to understand the hydration sphere structure of the metal ion of interest. For any quantum computation, the structure of the system under study has to be considered first. The nonahydrated structure of Gd^{3+} ion has been reported earlier using EXAFS [31]. Hence, we have considered nona-hydrated cluster of Gd^{3+} ion instead of searching for all possible structures. The structure of $(Gd^{3+}(H_2O)_9)$ is displayed in Fig. 1.

The calculated Gd-O distance (2.52) is found to be well matched with the EXAFS data (2.39)[31]. The corresponding IR frequency is also presented in Fig.1. The first peak arises due to the Gd-O bond and the remaining three are the signatures of bending, symmetric and anti symmetric stretching of O-H bond respectively. Three crown ethers namely DCH18C6, B15C5 and DB18C6 were used in the complexation studies of Gd^{3+} ion. The optimized structures of B15C5, DB18C6 and DCH18C6 and their complexes with Gd^{3+} ion are given in Fig.2. The reported ionic radii of Gd^{3+} ion is 2.16 . From the structural parameters it is found that the metal ion oxygen bond distance is found to be smaller in case B15C5 (2.368) as compared to DCH18C6 (2.402) and DB18C6 (2.625). Furthermore, the position of Gd^{3+} ion with respect to mean plane is displayed in Fig.2.

The calculated ΔE and ΔG of Gd^{3+} ion with the crown ethers both in gas and solvent phases are given in Table.1. The ΔE shows the order DCH18C6>DB18C6>B15C5. The ΔG in the gas phase also portrays similar trend of binding. Meanwhile, solvent phase calculations show the order DCH18C6>B15C5> DB18C6. This is because the solvation free energy of B15C5-Gd^{3+} complex is much
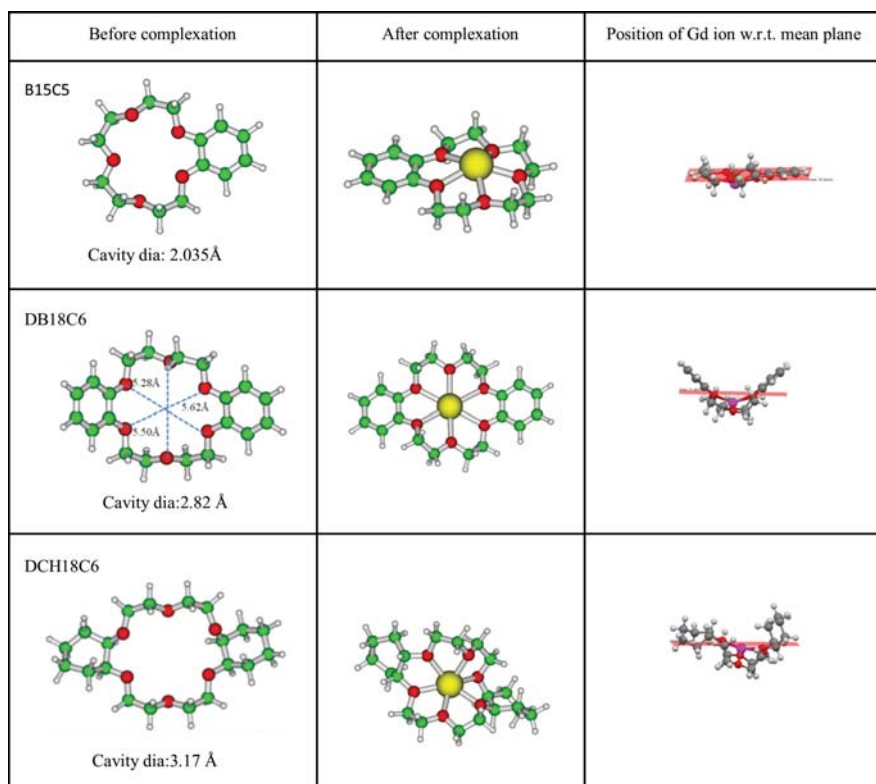
Fig. 2: Optimized structures of B15C5, DB18C6 and DCH18C6 and their complexes with Gd³⁺ ion

is considered to be promising for enrichment. But, in order to get considerable amount of enriched isotopes, the ligand should be grafted on solid matrix and then the separation should be carried out in columnar mode. To meet these criteria, DB18C6 is grafted on CMPS resin. In order to keep the molecular system computationally tractable, only one DB18C6 was anchored on repeated monomeric unit of CMPS. The optimized structure of Gd^{3+}-CMPS-DB18C6 is displayed in Fig.3. The predictability of computational protocol was validated by using the reported results of commercially available dowex resin with EDTA as complexing/enrichment agent. Furthermore, the calculated separation factor for 152/160 pair for Gd^{3+}-DCH18C6 ($\alpha=1.0012$) was found to be in good agreement with the experimental results ($\alpha=1.002$)[32] and thus confirms the acceptability of the present method of computation.

higher than DB18C6-Gd^{3+}. However, DCH18C6 was found to have more free energy of extraction.

The RPFR of Gd isotopic pair of 155/160 was found to be higher than 157/160 pair as shown in Table 2. The values of RPFR and α for hydrated Gd^{3+} ion and complexes of Gd^{3+} with various crown ligands were computed. In the case of dowex resin, observed separation factors are 1.000102 and 1.000086 for isotopic pairs of 155/160 and 157/160 respectively which are close to the experimental values of 1.000064 and 1.000040[11]. The separation factor for 155/160 pair is found to be higher compared to the 157/160 pair, due to a larger mass difference (Δm) in the case of 155/160 pair. The results show that α value with DB18C6 is higher compared to B15C5, DCH18C6. In view of comparatively higher α, DB18C6
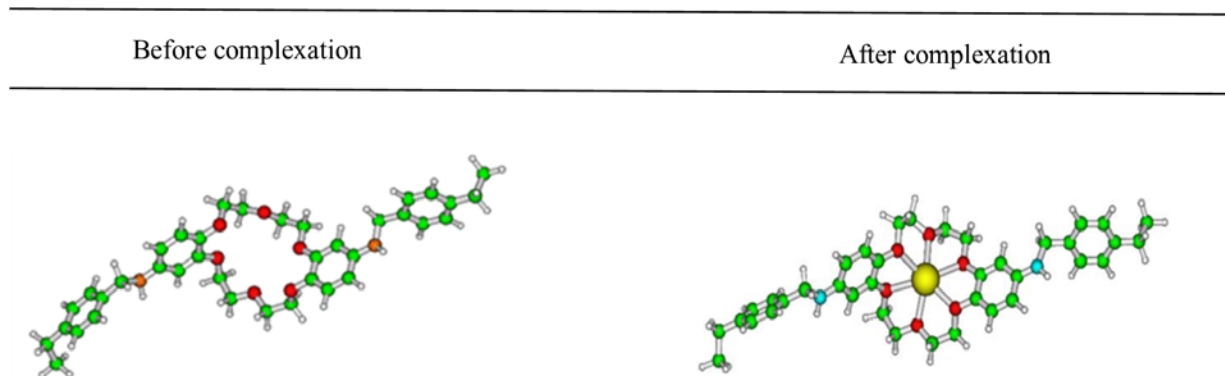
Experiments

Separation of Gadolinium Isotopes Using Solvent Extraction

$GdCl_3$ solution (0.03M) was used as the aqueous phase. The organic phase was 0.1M solution of B15C5, DB18C6 and DCH18C6 in nitrobenzene. 5 mL of each was mixed and then stirred for 1 hr in a magnetic stirrer. They were then allowed to stand for a day. The supernatant solution was used for concentration measurement. The concentration was determined by using ICP-MS and isotopic analysis was carried out using TIMS, developed by the Technical Physics Division, BARC. The distribution coefficient (K_d) of

Table 1: ΔE and ΔG of Gd^{3+} ion towards crown ethers and NBO charges on metal ion

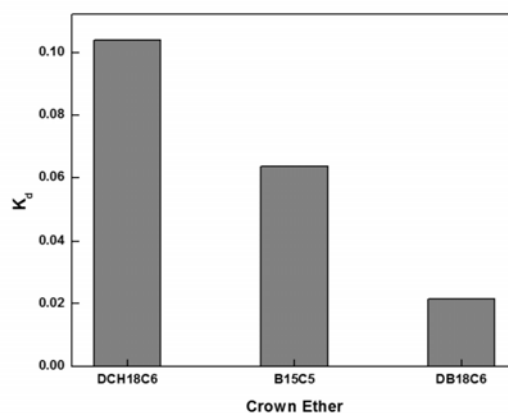|	Gd^{3+}-B15C5	Gd^{3+}-DB18C6	Gd^{3+}-DCH18C6
Charge on metal ion(gas)	2.098	1.651	2.110
Charge on metal ion(sol)	2.421	1.704	2.241
E(gas) (kJ/mol)	-1503.21	-1641.73	-1640.89
ΔG (gas) (kJ/mol)	-1454.96	-1590.01	-1603.57
ΔE (NB) (kJ/mol)	-122.87	-49.32	-124.72
ΔG (NB) (kJ/mol)	-74.62	2.40	-87.40
ΔS (kJ/mol K)	-0.145	-0.170	-0.141

Fig. 3: Optimized structures of complex of DB18C6 grafted CMPS with Gd³⁺ ion

metal ion, between organic and aqueous solution was determined using the following equation:

$$K_d = \frac{C_i - C_f}{C_f} \qquad (5)$$

Where C_i and C_f are the tinitial feed and final supernatant concentration of Gd³⁺ ion.

From Fig.4, it is found that the K_d value of Gd³⁺ follows the order DCH18C6 > B15C5 > DB18C6. From the molecular modelling calculations also, the same trend has been observed which further validates the computational results. So the present study thus validates the importance of computational study which can be used to elucidate the underlying mechanism for the metal ion selectivity (based only on theoretical route) and thus contributes to the design and screening of suitable ligands using computations. Although DB18C6 shows positive free energy from Quantum mechanics calculation, the experiments show the reverse picture. This anomaly may be addressed by appropriate consideration of spin state of the chemical species. The separation factor with DB18C6 was found to be higher compared to B15C5, DCH18C6 and also EDTA which shows that the use DB18C6 will be promising for future studies. So based on this, DB18C6 grafted to CMPS resin was synthesized in our lab and used for the isotope separation.
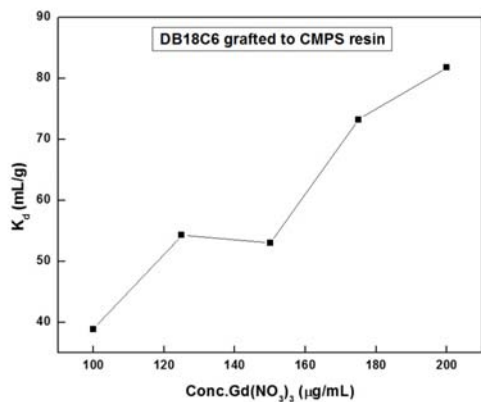

Fig. 4: K_d values of B15C5, DB18C6 and DCH18C6 in nitrobenzene

Distribution Coefficient Using Grafted Resin in Batch Method

The distribution coefficient (K_d) was evaluated using batch method. Each portion of 0.1g of dry (regenerated) CMPS grafted DB18C6 resin was weighed accurately and transferred into 50ml PP bottle. Then 10ml of Gd(NO₃)₃ solution of varying concentrations (100ppm to 200ppm) was added. The solutions were subjected to manual shaking at regular interval for 30min and kept overnight. The concentration of Gd³⁺ ion in the supernatant solutions

Table 2: RPFR and separation factor of Gd in water, EDTA and crown ether complexes

Complex of Gd³⁺	RPFR(f)		á$_{155/160}$	á$_{157/160}$
	Gd$_{155/160}$	Gd$_{157/160}$	=f$_{aq}$/f$_{comp}$	=f$_{aq}$/f$_{comp}$
9w	1.0024	1.0014		
EDTA	1.00151	1.000914	1.000102 (1.000064)	1.000086 (1.000040)
DCH18C6	1.001890	1.001083	1.000509	1.000317
DB18C6	1.000647	1.000391	1.001752	1.001009
B15C5	1.002016	1.001213	1.000383	1.000187
CMPS-DB18C6	1.001191	1.000712	1.0012	1.00068

Fig. 5: K_d values versus concentration of Gd³⁺ ion in separation with CMPS-DB18C6 resin

was determined using ICP-MS. The K_d of metal ion, between resin and solution, was determined using the following equation:

$$K_d = \left[\frac{C_i - C_f}{C_f} \right] \times \frac{V}{M} \left(ml / g \right) \qquad (6)$$

Where C_i = initial concentration of the solution, C_f = concentration of the supernatant solution, V = total volume of the solution (ml) and M = mass of dry resin (g).

The K_d values are plotted in Fig.5 indicating that the K_d value increases on increasing the concentration of metal ion with the resin.

Separation of Gadolinium Isotopes Using Column Chromatography

A breakthrough experiment was conducted in 6mm dia and 1m length column with CMPS-DB18C6 resin for Gd³⁺ ion using 0.005M Gd(NO₃)₃ (800ppm) at pH 6.50. The loaded Gd³⁺ was eluted using 0.5M HCl. The breakthrough curve is displayed in Fig.6a. From the breakthrough experiment it is observed that the adsorption capacity for Gd³⁺ ion is ~1mg/gm of resin.

Breakthrough curve indicates that the leakage of Gd³⁺ starts after volume reaches around 25 ml.

A study was also conducted by connecting two columns each of 6mm dia and 1m length column in series with CMPS-DB18C6 resin (Fig.7) for Gd³⁺ ion using 0.005M Gd(NO₃)₃. The pH was adjusted with NH₄OH to 6.50.The excess amount of Gd³⁺ was passed continuously to check the feasibility of isotope exchange. Samples were collected after every 20.0 ml turn, using automatic fraction collector, (Buchi make, Switzerland). The concentration of the samples was analyzed using ICP-MS and isotopic analysis of last few samples was carried out using TIMS. The loaded Gd³⁺ ion is further eluted using 0.5M HCl. The breakthrough curve is displayed in Fig.6b. The

Fig.7: Experimental setup of chromatographic separation of Gd isotopes

estimated values of isotope composition are presented in Tables 3 and 4.

The single stage separation factor, $\alpha = 1 + \varepsilon$ for each Gd isotope to defined as

$$\alpha = \frac{\left[\frac{^L Gd}{^H Gd} \right]_{resin}}{\left[\frac{^L Gd}{^H Gd} \right]_{sol}} \qquad (7)$$

Fig. 6: Breakthrough experiment using CMPS-DB18C6 resin for Gd³⁺ ion (a) Single column (b) double column

Table 3: The Gd isotopic ratios of samples collected in break through

Sample	Gd-155/158	Gd-157/158	Gd-155/160	Gd-157/160
Natural	0.59742±0.04%	0.63212±0.05%	0.67845±0.04%	0.71786±0.03%
B16	0.59940±0.03%	0.63410±0.02%	0.67786±0.03%	0.71710±0.02%
B18	0.59670±0.01%	0.63220±0.02%	0.67445±0.05%	0.71458±0.02%
B19	0.59831±0.03%	0.63236±0.01%	0.67695±0.01%	0.71547±0.01%
B20	0.59766±0.03%	0.61782±0.02%	0.67503±0.03%	0.69780±0.08%

Table 4: The Gd isotopic ratios of samples collected by eluting with HCl of sorbed Gadolinium

Sample	Gd-155/158	Gd-157/158	Gd-155/160	Gd-157/160
E1	0.59721±0.09%	0.631699±0.1%	0.67546±0.1%	0.71447±0.1%
E2	0.601814±0.002%	0.615184±0.1%	0.68576±0.5%	0.70100±0.5%
E4	0.5951±0.015%	0.631140.026%	0.67224±0.02%	0.71295±0.03%
E7	0.601023±0.02%	0.636394±0.1%	0.67879±0.04%	0.71874±0.1%

The separation coefficients, ε was calculated by using the isotopic enrichment curves of the front and rear boundaries according to the following equation [33].

$$\varepsilon = \sum \left(\frac{q_j}{QR_0} \right) \left[\frac{R_j - R_0}{1 - R_0} \right] \qquad (8)$$

where q is the amount of Gd in the sample fraction, Q is the total amount of sorbed Gd in the column packed resin, R_j is the isotopic ratio of $^{L}Gd/^{H}Gd$, and the subscripts j and o denote the fraction number and the original feed, respectively. In general, the isotope exchange reaction effectively proceeds and reaches the equilibrium between two phases of the solution and the resin at lower flow rate condition.

From the isotopic values in Table 3 the isotope separation coefficient was calculated. The separation coefficients, $\varepsilon \times 10^3$, were found to be 6.3, 8.9, 3.4, 9.7, 11.1 and 32.4 for 155/158, 156/158, 157/158, 155/160, 157/160 and 158/160 pairs respectively.

From the isotopic ratio measurements it was observed that slight isotopic separations have taken place in the resin bed. Since the adsorption capacity is low, more material is needed for the achievement of higher separation. Further study is in progress.

Conclusions

A combined molecular modelling and experimental study was performed for the feasibility of Gd isotope separation using crown ether functionalized resin. From the quantum calculations it was observed that the complexation of Gd^{3+} shows the order DCH18C6>B15C5> DB18C6 which was verified by performing a solvent extraction experiment. The calculated isotopic separation factor values show that DB18C6 is a promising candidate. So, CMPS-DB18C6 resin was chosen for the preliminary study of Gd isotopic separation. The adsorption capacity of the resin for Gd^{3+} was found to be 1mg/g. The separation coefficients ($\varepsilon \times 10^3$) were found to be 6.3, 3.4, 9.7 and 11.1 for 155/158, 157/158, 155/160 and 157/160 respectively and show promise for further study.

References

[1] Berglund, M., Wieser, M. E., *Pure and Applied Chemistry* 2009, *83*, 397-410.

[2] Sears, V. F., *Thermal-neutron scattering lengths and cross sections for condensed-matter research*, Chalk River Nuclear Laboratories Chalk River (Ontario) 1984.

[3] Abdollahi, M., Ahmadi, S. J., *Chemical Engineering and Processing: Process Intensification* 2014, *76*, 26-32.

[4] Artyukhov, A. A., Babichev, A. P., Knyasev, I. Y., Kravets, Y. M., *et al.*, *Nuclear Instruments and Methods in Physics Research Section A: Accelerators, Spectrometers, Detectors and Associated Equipment* 1997, *401*, 281-288.

[5] Egle, B. J., Hart, K. J., Aaron, W. S., *Journal of Radioanalytical and Nuclear Chemistry* 2014, *299*, 995-999.

[6] Keim, C. P., *Annual review of nuclear science* 1952, *1*, 263-292.

[7] Chen, J., Nomura, M., Fujii, Y., Kawakami, F., Okamoto, M., *Journal of Nuclear Science and Technology* 1992, *29*, 1086-1092.

[8] Hagiwara, Z., *Journal of Nuclear Science and Technology* 1969, *6*, 508-513.

[9]   Ismail, I., Matin, M., Nomura, M., Begum, S., Fujii, Y., *J. Ion Exch.* 2002, *13*, 40-45.

[10] Ismail, I., Nomura, M., Fujii, Y., *Journal of Nuclear Science and Technology* 1998, *35*, 801-807.

[11] Ismail, I. M., Fukami, A., Nomura, M., Fujii, Y., *Analytical Chemistry* 2000, *72*, 2841-2845.

[12] Ismail, I. M., Nomura, M., Fujii, Y., *Journal of Chromatography A* 1998, *808*, 185-191.

[13] Zhang, Y. H., Gunji, S., Nomura, M., Fujii, Y., Oi, T., *Journal of Chromatography A* 2005, *1069*, 133-139.

[14] Zhang, Y. H., Nomura, M., Aida, M., Fujii, Y., *Journal of Chromatography A* 2003, *989*, 175-182.

[15] Lehn, J. M., Sauvage, J. P., *Journal of the American Chemical Society* 1975, *97*, 6700-6707.

[16] Christensen, J. J., Eatough, D. J., Izatt, R. M., *Rev* 1974, *74*, 351.

[17] VAgtle, F., Weber, E., *Angew. Chem* 1974, *86*, 727.

[18] Jepson, B. E., DeWitt, R., *Journal of Inorganic and Nuclear Chemistry* 1976, *38*, 1175-1177.

[19] Heumann, K. G., *Organic Chemistry*, Springer 1985, pp. 77-132.

[20] Ali, S. M., Boda, A., Shenoy, K. T., Shenoi, M. R. K., *et al.*, *BARC Report* 2012, *R/005*, 1-60.

[21] Boda, A., Ali, S. M., Shenoi, M. R. K., Rao, H., Ghosh, S. K., *BARC REPORT* 2011, *I/011*, 1-24.

[22] Arora, S. K., Boda, A., Joshi, J. M., Singha Deb, A. K., *et al.*, *Proceedings of the DAE-BRNS biennial symposium on emerging trends in separation science and technology* 2014.

[23] Boda, A., Singha Deb, A. K., Ali, S. M., Shenoy, K. T., Ghosh, S. K., *American Institute of Physics Conference Series* 2014, pp. 1065-1067.

[24] Singha Deb, A. K., Ali, S. M., Shenoy, K. T., Ghosh, S. K., *Journal of Chemical & Engineering Data* 2014, *59*, 2472-2484.

[25] Ahlrichs, R., Bar, M., Haser, M., Horn, H., Kolmel, C., *Chem. Phys. Letters* 1989, *162*, 165.

[26] Becke, A. D., *Physical Review A* 1988, *38*, 3098.

[27] Becke, A. D., *The Journal of Chemical Physics* 1993, *98*, 1372-1377.

[28] Lee, C., Yang, W., Parr, R. G., *Physical Review B* 1988, *37*, 785.

[29] Urey, H. C., Rittenberg, D., *The Journal of Chemical Physics* 1933, *1*, 137-143.

[30] Bigeleisen, J., *Journal of the American Chemical Society* 1996, *118*, 3676-3680.

[31] Persson, I., D'Angelo, P., De Panfilis, S., SandstrAm, M., Eriksson, L., *Chemistry-A European Journal* 2008, *14*, 3056-3066.

[32] Fujii, T., Yamamoto, T., Inagawa, J., Gunji, K., *et al.*, *Solvent extraction and ion exchange* 1999, *17*, 1219-1229.

[33] Spedding, F. H., Powell, T. E., Svec, H. J., *Journal of the American Chemical Society* 1955, *77*, 6125-6132.

Preparation and Validation of Gas Sealed High Isotopic Purity Heavy Water Reference Standards

**K. Dhole, T. Vasudevan, P.R. Dani, S. Ramabhadran,
R. D. Ghadigaonkar and A. Datta**
Research Reactor Services Division
and
A.V. Gandhi and N.D. Mathur
Heavy Water Plant, Baroda, Vadodara

Abstract

The method for preparation of helium gas sealed high isotopic purity heavy water (D_2O) reference standards on a large scale has been amply demonstrated. The percentage purity of the reference standards has been estimated employing Fourier-Transform Infrared (FT-IR) method standardized with certified D_2O standard and confirmed by validation using the same method with supplementary certified standard having its purity value declared from a different method – Fourier-Transform Nuclear Magnetic Resonance (FT-NMR) spectroscopy, each of the certified standards having an accuracy of $\pm$ 0.01 wt.%. The work has also been extended in the preparation of high purity reference standards (99.86 wt.%, 99.90 wt.% and 99.96 wt.%) with an accuracy of $\pm$ 0.01 wt.% in stainless steel storage-containers (total 15 Nos.) in collaboration with Heavy Water Plant (HWP) laboratory, Baroda, Vadodara. The standards prepared are extremely useful for day-to-day quality control of product D_2O as well as certifying the quality of export consignments from different HWPs. This also helps all the heavy water plant laboratories in India to analyze high grade heavy water samples with same level of accuracy and reproducibility.
Keywords: D_2O; Heavy Water; H_2O; Light Water; Isotopic purity, Fourier-Transform Infrared spectroscopy; IR

Introduction

The nuclear power program in India has been conceived on optimum utilization of domestic uranium reserves for Pressurized Heavy Water Reactors (PHWRs) [1]. The inherent advantage of heavy water (D_2O) with low neutron absorption and effective moderation facilitates the use of natural uranium (0.7% ^{235}U) as fuel in PHWRs. D_2O is basically used as a neutron moderator and coolant in PHWRs and NRU type research reactors. In the Indian context, production of heavy water and the estimation of its isotopic purity are important aspects because of its extensive use in all existing and future PHWRs. The specification for reactor grade (> 99.78 wt.%) high isotopic purity heavy water is quite rigid; a slight change in the concentration of deuterium in heavy water can alter the neutron availability in the reactor. The lowering of deuterium concentration of heavy water *i.e.* downgradation of D_2O in a reactor core results in loss of neutron population *viz.* reactivity [2, 3]. Likewise, immense care is needed while handling heavy water standards and samples because of their extreme hygroscopic nature. The storage of large quantity of heavy water standard is also equally indispensable, particularly for its high isotopic purity. Hence, stainless steel containers with helium blanket have been considered for long term storage in the process of making high purity reference standards. A series of steps have been followed here taking adequate care and protection from air ingress during the entire procedure.
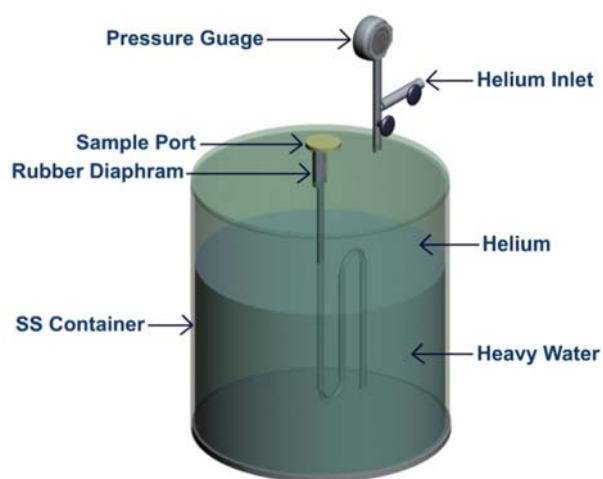
Prior to the estimation of isotopic concentration of heavy water for its quality assurance, it may be remembered that D_2O is not synthesized from pure substances, rather it is prepared by separation techniques for its plant scale requirements. It is not possible to have primary D_2O standards in a strict sense. Universal standards are available only at the low (0-1 wt.%) concentration range. There are no universal standards available in the middle (1-99.5 wt.%) and high (> 99.5 wt.%) concentration ranges. Furthermore, literature suggests that the isotopic purity of heavy water can be determined with various analytical techniques [4-8], each being sensitive at different concentration ranges of D_2O. Nevertheless, most of the techniques are not absolute except some cumbersome and time-consuming methods based on density measurements. Hence, quantification and validation of reference standards is solely based on multiple measurements in a number of laboratories.

The present work reports the preparation of helium gas sealed heavy water reference standards on a large scale in the high concentration range and quantify them on application of Fourier-Transform Infrared (FT-IR) spectroscopy - one of the appropriate analytical techniques. In addition, these large-scale high purity reference standards are to be validated by the same FT-IR method (fast & precise technique) calibrated with supplementary certified D_2O standard having its purity value declared from a substitute method – Fourier-Transform Nuclear Magnetic Resonance (FT-NMR) spectroscopy.

Experimental

Materials and method

All the stainless steel containers were fabricated with SS-304 material for long term storage of high concentration heavy water. Each container was provided with a sample port with neoprene rubber diaphragm as shown in Fig. 1. Helium was taken as blanket gas which is to be filled through the helium inlet valve. The folded tube below the sampling port provides   a long diffusion path barrier if a trace of moist air enters through the diaphragm. The high purity D_2O (99.97 wt.%) was supplied by heavy water production plant, DAE. Ultra pure water (>18 MÙ-cm, Milli-Q) was used as diluting agent in the preparation of reference standards at different purity levels.

Fig.1. Design of stainless steel container for storage of high purity heavy water reference standard

Conditioning of stainless steel containers

Initially, Dye penetrant inspection (DPI) test was carried out to check surface-breaking defects in all the steel containers as per procedure qualified to ASME Section V [9]. All the containers were further qualified employing the hydrostatic test on application of test

pressure 2.0 kg/cm^2 (g) for 30 minutes so as to maintain their safety standards and durability over time. Clean up of impurities inside the containers was performed by rinsing them thoroughly with de-mineralized water followed by acetone (AR Grade) to satisfactory level. Subsequently, they were taken into drying with hot air followed by dry helium gas to allow all the acetone vapors to get released. The dew point test for each of the containers has was also conducted to ensure the complete dryness. Final dew point after purging with Ultra High Purity (UHP) nitrogen was about - 40^{0}C. Lastly leak test / pressure test has been done for each of them by introducing dry helium gas using moisture trap through the helium inlet valve and keeping them sealed to a certain pressure of 1.1 kg/cm^2 (g) for about 10 days. Absence of any pressure drop ensured that the containers were leak-proof. Once the containers tested leak proof, they were all set to be filled with high purity heavy water.

Filling up of stainless steel containers

To prepare a standard at a desired value of isotopic purity, appropriate amount of ultra-pure H_2O was mixed with weighed quantity of high grade D_2O at its known concentration in a completely desiccated plastic container separately and then purity analysis of the resultant water was carried out by FT-IR method before transferring it to a storage - steel container. A dry stainless steel tube, fitted at one end by a threaded stopper compatible to the sample port of the steel container and the other end connected to a dry rubber tube, was used in transferring the resultant heavy water from plastic container to steel container in order to minimize the aerial contact of D_2O. About 15 kg of the resultant heavy water was transferred into a storage container through D_2O rinsed rubber tube connected to the stainless steel tube-fitting with the help of nitrogen pressure. The storage steel container was closed and blanketed with helium gas to a pressure of 0.7 kg/cm^2(g). To fill other stainless steel containers with heavy water at different desired values of isotopic purity, the same procedure was followed. Once containers are filled with high isotopic purity heavy water, any downgrading of D_2O in the process of transfer and subsequent storage for long duration needs to be confirmed.

Infra red analysis of heavy water isotopic purity

To ensure no downgradation during the process of transfer and subsequent storage of high purity D_2O in stainless steel containers for long period as well, samples were collected from storage-containers with standard hypodermic dry needle and luer-lock syringe

by puncturing the rubber diaphragm of the sample port and analyzed for isotopic purity employing FT-IR method at regular intervals. The diaphragm is self-sealing when the needle is withdrawn. Fresh calibration was made with certified D_2O standard. Finally the isotopic concentration of D_2O in the reference standards prepared was further validated by making a new calibration with the same FT-IR method using supplementary certified standard. All the FT-IR spectra were collected at room temperature (25°C) against air background on a FT-IR spectrometer equipped with high-intensity ceramic light source and DLATGS detector using a CaF_2-transmission cell of 0.5 mm path length by transferring each representative sample from storage container. Each FT-IR spectrum corresponds to an accumulation of 16 scans with a resolution of 4 cm^{-1}. For analytical purpose, all the spectra were linearly off-set at ~3400 cm^{-1} for IR absorption by H_2O + HDO as shown in Fig. 2 and the decrease in absorbance with increase in concentration of D_2O has been recorded. Calibration error for the response of Infra-Red instrument with heavy water standards has also been monitored on a regular basis. The process for analysis and validation of these large-scale reference standards was continued for six months to ensure that the purity of reference standards remained unchanged at respective desired values without any downgradation. It is also to be noted here that the pressure of helium blanket gas was maintained from the commencement of the process of confirmation till their final use at 0.7 kg/cm^2 (g).
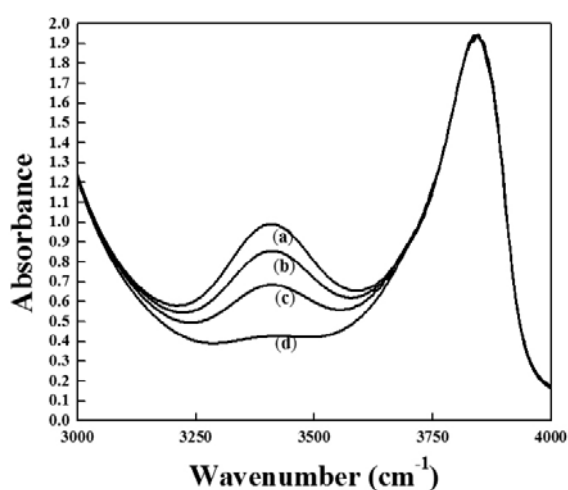
Results and Discussion

Quantification and validation of reference standard

The measurements of IR absorbance were repeated several times and the reproducibility of the measurements was found to be $\pm$ 0.002. Initially, the concentrations of large-scale reference standards, made at desired isotopic purity values of 99.82 wt.% & 99.86 wt.%, were estimated from a linear calibration with the correlation coefficient (R^2) of 0.99952 in the range of 99.82 – 99.86 wt.% as shown in Fig. 3. This calibration was generated from the certified D_2O standard, declared with purity value of 99.86 wt.% ($\pm$ 0.01) based on density measurement. The other large-scale D_2O reference standard prepared at desired purity value of 99.96 wt.% was analyzed in an alternate way by lowering the concentration of its representative sample in the above range. Subsequently, the isotopic concentrations of these three large-scale reference standards were confirmed by validation from a new calibration with the correlation coefficient (R^2) of 0.99946 in the range of 99.82–99.96 wt.% as shown in Fig. 4. This new calibration was produced from the supplementary certified standard, having its purity of 99.98 wt.% ($\pm$ 0.01) declared by a substitute method - FT-NMR spectroscopy. Furthermore, prior to use as working standards for quality assurance, the evaluation of uncertainty in isotopic purity estimation was made by these large-scale reference standards together with certified standards on application of linear regression model based on Gaussian distribution of variables. The resulting equation is given by

$$x\left(\text{wt.%}\right) = - 0.24955 \times y\left(\text{Absorbance}\right) + 100.06849 \quad (1)$$

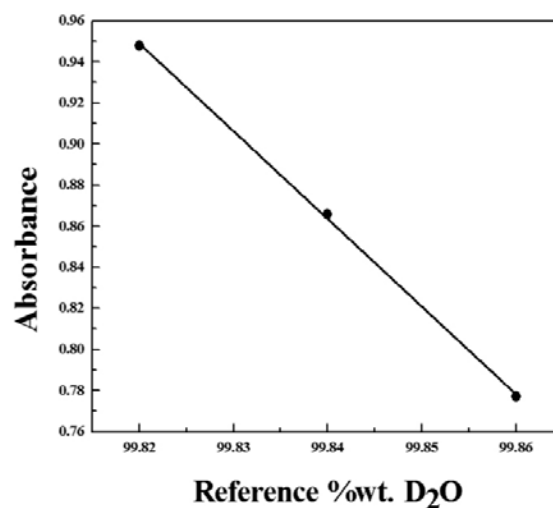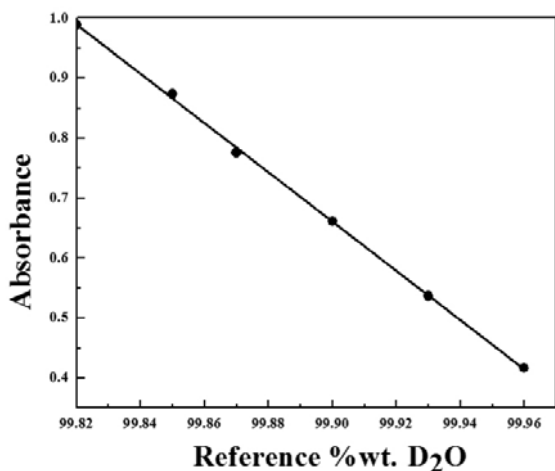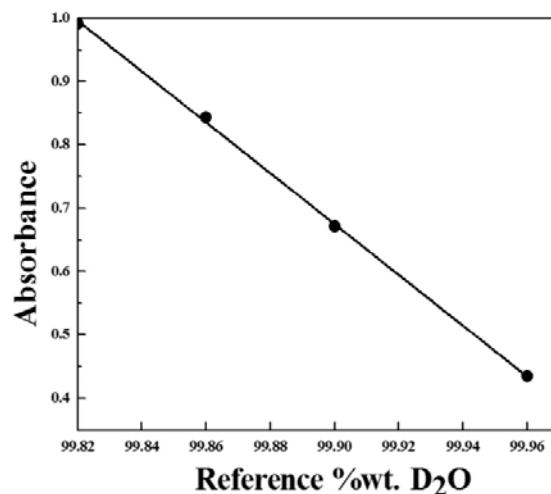Fig. 2: Absorption spectra of H₂O + HDO: (a) 99.82 wt.%; (b) 99.86 wt.%; (c) 99.90 wt.%; (d) 99.96 wt.%.

Fig. 3: Linear calibration of absorbance as a function of isotopic purity in the range of 99.82 – 99.86 wt.% generated from certified standard

Fig. 4: Linear calibration of absorbance as a function of isotopic purity in the range of 99.82 – 99.96 wt.% generated from supplementary certified standard

with the correlation coefficient (R^2) of 0.99970. Then the resulting standard uncertainty (SU) in isotopic purity estimation was calculated using the following equation:

$$(2)$$

where x_R is respective reference wt.% concentration of D_2O, N denotes number of reference standards and x_{Th} corresponds to theoretically calculated wt.% data using Eq.(1) at each measured value of absorbance. The achieved SU viz. the reproducibility of isotopic purity estimation is found to be $\pm$ 0.002 wt.%. The prolonged analysis followed by further validation ensures the percentage purity of reference standards prepared at their respective desired values. These standards prepared on a large scale, about 15 kg each, with isotopic purity values of 99.82 wt.%, 99.86 wt.% and 99.96 wt.% are now employed as working standards in high purity range. Furthermore, these high purity working standards were employed as reference standards for quantification and validation of another set of D_2O standards (99.86 wt.%, 99.90 wt.% and 99.96 wt.%), about 8 kg each, jointly prepared with Heavy Water Plant (HWP) laboratory, Boroda, following the procedure described above. A separate linear calibration with the correlation coefficient (R^2) of 0.99941 in the range of 99.82 – 99.96 wt.% as shown in Fig. 5 has been produced employing the above working standards for the purity analysis of the new set of D_2O reference standards to obligate them with same degree of accuracy and reproducibility.

Fig. 5: Linear calibration of absorbance as a function of isotopic purity in the range of 99.82 – 99.96 wt.% generated from large-scale working standards prepared

Conclusion

Helium gas sealed high isotopic purity heavy water reference standards have been prepared in stainless still storage containers. Initially three reference standards (99.82 wt.%, 99.86 wt.% and 99.96 wt.%), 15kg each, have been prepared and estimated their respective purity values employing FT-IR method standardized with certified D_2O standard, stated with purity value based on density measurement. This has been followed by validation of these reference standards using the same FT-IR method with supplementary certified D_2O standard, having its purity value declared from a substitute method – FT-NMR spectroscopy. Each of the certified standards considered here has an accuracy of $\pm$ 0.01 wt.%. In addition, the same procedure for preparation and validation has been well employed using these reference standards as working standards to declare the isotopic purity values of another set of reference standards (99.86 wt.%, 99.90 wt.% and 99.96 wt.%) with accuracy of $\pm$ 0.01 wt.% prepared in stainless steel storage containers (total 15 Nos.), 8 kg each, (Table 1) in collaboration with Heavy Water Plant (HWP), Baroda. The standards made here are extremely useful for day-to-day quality control of product heavy water as well as certifying the quality of export consignments from different HWPs. This also helps all the heavy water plant laboratories in India to analyze high grade heavy water samples with same level of accuracy and reproducibility.

Table 1: Purity & wt. of Reference Standards dispatched

Heavy Water Plants (HWPs)	No of Standards	Weight of Heavy Water Reference Standards (Kg.)		
		99.86 wt.%	99.90 wt.%	99.96 wt.%
Manuguru	1	8	8	8
Hazira	1	8	8	8
Baroda	1	8	8	8
Kota	1	8	8	8
Thal	1	8	8	8

Acknowledgement

References

1. J.S. Bharj, R.R. Sahaya, D. Datta and S.P. Dharne, ICAPP, p. 1134-1142 (2006).
2. H.K. Rae, Separation of Hydrogen Isotopes, ACS Symposium Series 68, (1978).
3. S.Glasstone and A. Sesonske, Nuclear Reactor Engineering, third ed. CBS Publishers & Distributors, Shahdara, Delhi, India , (1986).
4. R.D. Jr Kimbrough and R.W. Askins, *Analytical Chemistry* 41(8), 1147-1148, (1969).
5. S. Han, H. Chung and J.W. Han, *Analyst* 130(5), 745-749, (2005).
6. W.H. Stevens, J.G. Bayly, W. Thurston and V.B. Kartha, Atomic Energy Canada Limited, Report No. AECL-1391, (1961).
7. R. P. Shukla and D.V. Udupa, *Optics & Laser Technology*, 32(5), 355-360, (2000).
8. K. Dhole, M. Roy, S. Ghosh, A. Datta, M.K. Tripathy and H. Bose, *Ann Nucl Energy*, 55, 116, (2013).
9. ASME, Boiler and Pressure Vessel Code, Section V, Art. 6, *Liquid Penetrant Examination*, p.128-134 (2011).

Thomson parabola: A High Resolution Ion Spectrometer

S. Chaurasia, Vinay Rastogi and D. S. Munda
High Pressure & Synchrotron Radiation Physics Division

and

R. K. Bhatia and V. Nataraju
Technical Physics Division

Abstract

A compact high resolution and high dispersion Thomson parabola ion spectrometer (TPS) comprising of Time-of-Flight diagnostics has been developed for simultaneously resolving protons and low-Z ions of energy from 1keV/nucleon to 1MeV/nucleon and incorporated in the Laser plasma experimental chamber. The ion spectrometer was optimized with carbon target. The carbon ions of charge states 1+ to 6+ were measured in the energy range from 3 keV to 300 keV, which were verified by time-of-flight measurements. The energy resolution (E/dE) of TPS was achieved up to 50 depending on the energy and charge states of the ions. The experimental results were in fairly good agreement with the theoretical simulations.

Introduction

In the past several years, Thomson parabola ion spectrometer has become a promising ion diagnostic tool as it provides information of energy, momentum, charge-to-mass ratio, etc., simultaneously. It has been used for study of ion sources such as collective ion accelerators[1], laser-produced ion source (LIS)[2], Ion diodes[3] etc. An LIS is an option for injection system of heavy ions for the Large Hadron Collider at CERN. In the LIS, all solid and gaseous elements can be ionized. Depending on the parameters of the laser used, LIS can deliver ions with charge states from Z =1 (like in laser mass spectrometry), up to Z>50, atomic masses from $A=1$ up to $A=200$ amu and energies from hundreds of eVs up to several MeVs. Also, for estimation of laser-produced plasma parameters, ion parameter measurements are very important. Thomson parabola is a very useful diagnostic tool, since it provides the distribution of particle as a function of energy, momentum and charge-to-mass ratio simultaneously.

Working Principle of TPS

Unlike normal mass spectrometer, TPS is comprised of both electric and magnetic fields. Since in the laser produced ion source we get various charge states and each charge carrying vast energy spectrum, using one field will not suffice to differentiate all charge states. The working principle of Thomson parabola employs the use of magnetic field and electric field, oriented parallel to each other and perpendicular to the ion beam propagation direction. The ions are deflected by the Lorentz force $\vec{F} = q(\vec{E} + \vec{v} \times \vec{B})$, parallel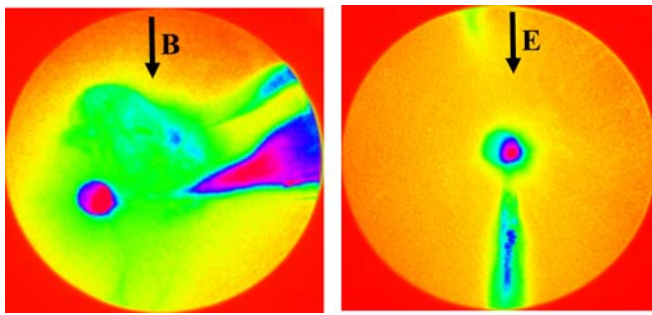 to the electric field (E) and perpendicular to the magnetic field (B), where, v is the velocity of ions, q = Ze is the ion charge, where Z is ions charge state and e is the electric charge. For an ideal Thomson parabola, considering non-relativistic particles, the deflection of charge particle in the magnetic and electric field can be shown in Figs.1a & b and can be written as

$$x(detector) = \alpha.\frac{ZeB}{(mE_k)^{1/2}} \text{ and } y(detector) = \beta.\frac{ZeV}{E_k} \qquad (1)$$

where $\alpha = \frac{l_1}{2} + l_2 + l_3 + l_4$, and $\beta = l_3\left(\frac{l_3}{2} + l_4\right)\Big/2d$, m is the mass of the ion, E_k is kinetic energy of the ion, and V is the voltage difference between two plates, B is magnetic field strength. $l_1, l_2, l_3,$ and l_4 are the lengths of the magnetic shoes, spacing between magnet and electrode, length of the electrode and distance between electrode and detector respectively. From equation (1), it is clear that, for a fixed magnetic field (i.e. B = constant), higher the charge states higher will be the ion deflection. Also, higher kinetic energy ions will see lower deflection. Similarly, it can be seen from the equation (1) that, higher charge state and lower kinetic energy ions will see more deflection in the electric field.

Combining the magnetic and electric fields together results in the parabola for each charge state on the detector as shown, in Fig. 2d and the equation of parabola can be written as

$$y(detector) = \left[\left(\frac{\beta}{\alpha^2}\right).\left(\frac{m}{Z}\right).\frac{1}{e}.\frac{V}{B^2}\right]x^2(detector) \qquad (2)$$

Fig. 1: (a) The deflection of charge particle in the magnetic and (b) Electric field

From the equation, it is inferred that, the ions of identical mass/charge (m/Z) ratios are arranged in the same parabola, for the fixed values of V and B. The points of intersection of parabolas with the line x/y = constant, that is the line passing the origin of the coordinates, correspond to ions of fixed velocity and be written as $v = \sqrt{2}(\beta/\alpha)(V/B)(x/y)$ and is independent of the (m/z) ratio called as iso-velocity line (shown in Fig. 2d, blue line). From equation (1) a few important parameters associated with the ions can be derived such as momentum per unit charge from first part of equation (1) and can be written as
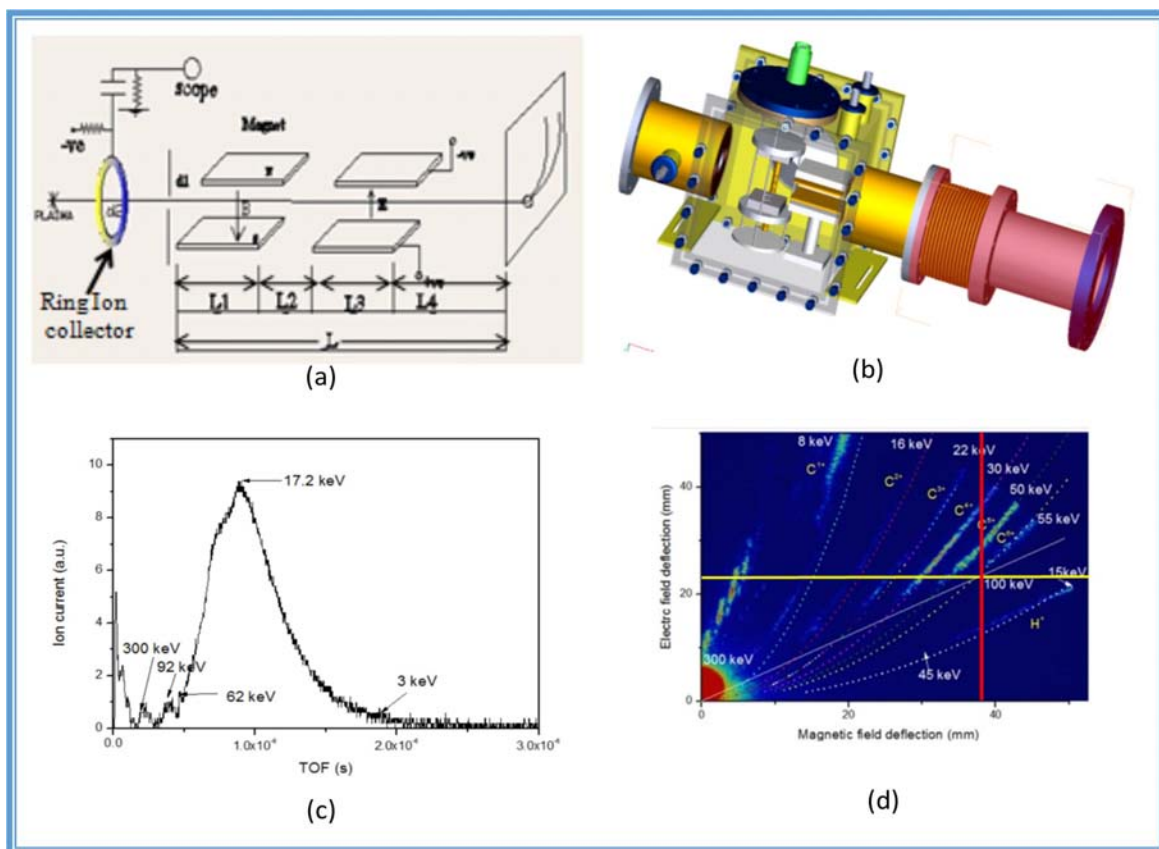
$$p/Z_i = \sqrt{2}\,\alpha\,eB/x \tag{3}$$

which is inversely proportional to magnetic deflection (x) and independent of the electric deflection. Any vertical line x = constant (red line)(Fig.2d) corresponds to a constant momentum per charge. Similarly, the kinetic energy per unit charge can be written as

$$E_k/Z_i = \beta eV/y \tag{4}$$

which depends only on the electric field deflection any ions on the vertical line y = constant (yellow colour) have a constant energy per charge.

Thomson parabola with time-of-flight (TOF)

An ion spectrometer, composing of a time-of-flight spectrometer (TOFS) and a Thomson parabola spectrometer (TPS), has been developed to measure energy spectra and to analyze species of laser-driven ions as shown in Figs. 2a (schematic) and 2b (3D view). The two spectrometers (ie TPS & TOFS) can be operated simultaneously, to compare independently measured data and to combine advantages of each spectrometer. Real-time and shot-to-shot characterizations have been possible with the TOFS, and species of ions can be analyzed with the TPS. The two spectrometers show very good agreement as can be seen from Figs. 2c and 2d.

Fig. 2: (a) Schematic of Thomson parabola ion spectrometer (b) Design of TPS (c) Ion collector signal and (d) Thomson parabola record of the graphite plasma.
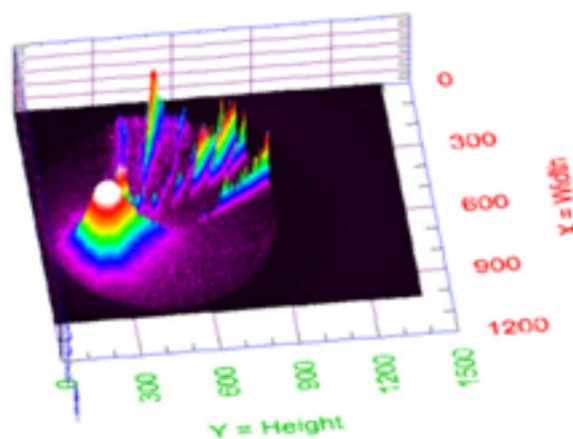
The ring ion collector functions as a Faraday cup, with the difference that, it is not completely destructive. The ion collector is a ring with a 2 mm aperture in the centre. When the ion collector is mounted in the path of a particle beam, the central part of the beam will pass through the collector and the outer part will be collected. This collector acts as the beam intensity control and is also used for collimation (ion beam shaping) in the entrance of the Thomson parabola assembly. TOF is one way of measuring complete energy spectrum of ions in a single shot. The resolution is poor and cannot separate charge states. Thomson Parabola Spectrometer has a limitation of measuring the energy spectrum, the constraint being enforced by the detector size. Hence, to get the optimum result coupling of TOF and Thomson parabola spectrometer is beneficial.

The Thomson parabola unit was installed in the experimental chamber at an angle of 45^0 with respect to the port used for the laser beam. The experiment was performed on our 30 J Nd Glass laser system. The graphite targets were mounted on the 4 axis motorized translational stage in the vacuum chamber evacuated to 5×10^{-6} mbar pressure. The laser was focused on the target to a diameter of 100 μm such that, laser intensity was about 5×10^{13} -7×10^{14} W/cm^2. The target was rotated by 45 degree with respect to the laser beam so that maximum ion flux will reach the ion spectrometer. Since laser-produced ion source from solid target is spread over 2π, shaping of ion beam into a very small size is required to get high-resolution spectrum and charge separation. The shaping of the ion beams was done with the help of 2 mm aperture in ring type ion collector and a pinhole of diameter 80 to 150 μm kept at 2mm before the magnetic shoes. Two permanent magnets were mounted inside the housing through linear magnetic feed-throughs attached with micrometer movements for the adjustment of the magnetic field by changing the spacing between the magnets. The magnetic field can be varied from 150 Gauss to 2 kGauss. Two copper electrodes were connected with −ve and +ve polarity of electric field. The voltage difference between two electrodes can be varied from 0 V to 10 kV.

A 75 mm diameter two-stage MCP detector, with phosphor screen in Chevron configuration is placed at a distance of D=380 mm from the end of the electrodes. The parabola recorded for the graphite plasma at laser intensity of 2×10^{14} W/cm^2 is shown in Fig. 2d. The magnetic and electric fields for this laser shot were kept at 310 Gauss and 300 V, respectively. The experimental observation was in fairly

good agreement with the theoretical simulation done by the SIMION code (which is discussed briefly in next section) for the same magnetic and electric field. There was a slight deviation of theoretical result with experimental observation for C^{1+} ions energy spectrum, which may be due to fringe field effect. From Fig. 2d, it can be seen that protons of energy range 15 keV to 45 keV are also present and this is attributed to the impurity on the targets. From the image, it is observed that all the ions start with 100 keV energy on the parabola except C^{1+}, which shows upto 300 keV energy. The range of the energy spectrum recorded on the parabola was also measured with ion collector as shown in Fig. 2c.

In case of calibrated MCP on ion accelerator, the flux of each charge state of a particular energy can be measured. The brightness of the parabola traces on the MCP is proportional to the flux of the ions. The 3D plot of the carbon ion spectrum recorded for the laser intensity 2×10^{14} W/cm^2 on MCP is shown in Fig. 3. Higher the intensity of the parabola, higher will be the flux.

Fig. 3: 3D view of ion spectrum enable to measure qualitatively the flux of ions of particular energy

Computer simulations

The simulations were carried out using SIMION 7.0 software. This software uses finite difference method to calculate the field values at grid points generated around the electrodes. Geometry of the magnet and the electrostatic analyzer (ESA) were created as a separate potential array and coupled together in a single ion optical bench. The size of each pole of the magnet system was taken as 50 mm (l) x 50 mm (w) x 10 mm (h) with a pole gap of 6 mm. For ESA, two rectangular electrodes with dimensions of 80 mm (l) x 50 mm (w) were placed parallel to each other with

a gap of around 16 mm. Another electrode plate with pinhole (0.08 - 0.15 mm diameter) was generated at a distance of around 2 mm from the magnet entry position. Ions were generated in different groups of charge states with required mass and energy in the range of 3 keV to 1 MeV. These ions were passed through magnetic and electric fields sequentially and the ions trajectories were truncated at a distance of 600 mm (detector distance) from the pinhole. The simulation results, shown with dotted line in Fig. 2d, are well matched with experiments.

Conclusions

A high resolution/high dispersion ion spectrometer comprising of a ring type ion collector for time-of-flight measurements and Thomson parabola with varying magnetic and electric fields has been developed. The energy resolution (E/dE) of TPS achieved was up to 50 depending on the energy and charge states of the ions. The carbon ions of charge states 1+ to 6+ were measured in the energy range from 3 keV to 300 keV which have been also verified by time-of-flight measurement. Protons of energy ranging from 15 keV to 45 keV were also registered on the MCP. The design parameters and the experimental results are in fairly good agreement with the simulated results using SIMION code.

Acknowledgements

References

1. G. W. Kuswa, L. P. Bradley, and G. Yonas*, IEEE Trans. NucL Sci*. NS·20, 305 (1973).

2. D. C. Carroll, et al., *Nuclear Instruments and Methods in Physics Research Section A* 620, 23 (2010).

3. T. Ozaki, S. Miyamoto, F. Ogawa, A. Yoshinouchi, K. Imasaki, S. Nakai and C. Yamanaka, *J. Appl. Phys*. 54, 632 (1983).

Rural-Friendly
Drinking Water Purification Systems

Saly Thomas Panicker, P.K. Tewari and D. Goswami
Desalination Division

Abstract

Scarcity of safe drinking water is a real issue in coastal and rural areas. Drinking water with physical, chemical or biological contamination has harmful effects on human health. Surface water is normally affected with disease-causing organisms such as, bacteria, viruses, protozoa, parasitic worms etc. and ground water at certain locations contains high loads of dissolved salts. Membrane based technologies and systems provide one-step solution in such cases. While Ultra-filtration (UF) based systems are very effective in removing biological and other colloidal species, Reverse Osmosis (RO) is capable of removing dissolved salts to the extent that the total dissolved solids (TDS) of the product water can be brought down to potable limits (< 500 mg/l). UF and RO are pressure driven processes and hence they require energy in the form of electricity for pumping the contaminated feed water through the membranes. Remote locations and majority of Indian villages still do not have proper access to grid electricity. Off-grid systems which work on human energy or renewable energy are the only viable solutions to deal with such a situation. The Govt. of India provides medical aid in terms of services of medical staff & medicines freely to the under-privileged people. As most of the illnesses are water-borne, free supply of safe drinking water to them by installing these systems would be a preventive and healthier measure. This would not only improve the state of the rural community, but would also minimize spending by the public exchequer.

As part of the societal role of DAE/BARC under non-power application programme, the Desalination Division (DD), BARC has developed manually operable, rural-friendly water treatment units/systems which do not need electricity. If properly deployed and managed, they would be of real help to the most-deserving communities for obtaining safe drinking water. Knowhow of these systems is ready for transfer to interested entrepreneurs.

Introduction

Water is one of the essential elements which mother nature has given us free of cost. The available water could be contaminated due to geo-genic and/or anthropogenic factors. It should be noted that, there is no alternative for water other than water itself. As per World Health Organization (WHO) and Indian Standards (IS-10500), water is safe to drink if the water is clear and free of microorganisms and the total dissolved salt content is less than 500 mg/l (ppm). In rural areas, the open water bodies are highly infested and the normally reported brackishness in the ground water is in the range of 1000 – 3000 ppm.

Water treatment technologies such as, membrane based Ultrafiltration (UF) and Reverse Osmosis (RO) are available for removing dissolved & un-dissolved physical, chemical & biological contaminants. In general, the water treatment systems are compatible with urban/semi-.urban sectors, where proper infrastructures are available. Several remote and rural areas in India are not connected to the grid power network due to their remoteness or even if connected, the voltage available is not stable. Ironically, water

Fig. 1: Lifeline of majority of India. (1,2)

problems are more severe in such places and the people are surviving on unsafe and insufficient drinking water, risking their health (Fig. 1).
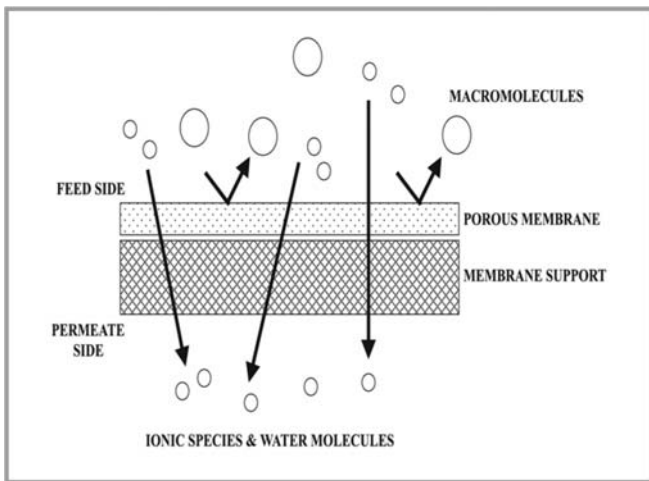
The rural-friendly water treatment systems developed by BARC consist of RO and UF systems integrated with manually driven pumps. Electrical pumps supported by solar photovoltaic (PV) panels also can be incorporated to act as standby or complementary system. The production capacity varies from 10 – 100 litres/hr (lph). As the energy cost is nil for operation, the purified water becomes more affordable by the

poor section of the society. These units can be effectively deployed in schools and small communities. They can be easily transported and would be of great help for people moving in desert/wilderness, as in the case of defence personnel, trekkers etc.

Technical Details of the Systems

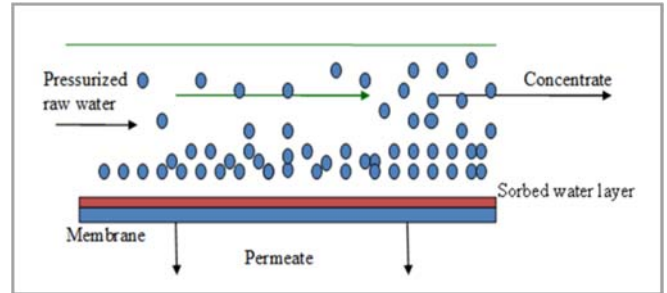### Ultrafiltration (UF) System

As shown in Fig. 2, in the process of Ultrafiltration, the suspended and colloidal particles including micro-organisms are filtered out by the membrane having 0.01 - 0.1 micron pore sizes (3). The raw feed water needs to be pressurized to push the water through the micro-pores of the membrane/s. Surface or well waters containing filterable/suspended contamination without excess salinity can be made fit for drinking by treating with UF alone.

Fig. 2:   Schematic Representation of Ultrafiltration

In the UF system, the feed water is passed through the membrane with the help of a DC pump directly connected to the PV panels (20 -40 W) without any batteries. The membrane material is polysulfone. Filtration is in dead-end mode. The feed may be pre-

treated by an activated carbon filter to remove undesired taste, odour, organics etc. The UF element is either a candle (70mm diameter & 220mm length) or in capillary (45 mm diameter & 300 mm length) form. Fig. 3 shows the process schematic of the UF system.
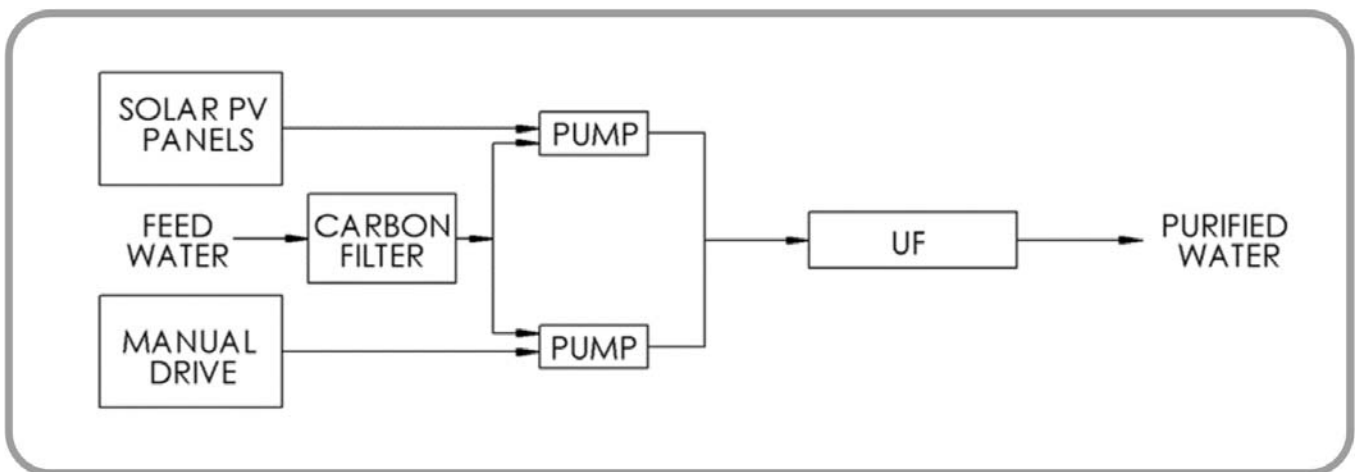

Fig. 4: Schematic Representation of Reverse Osmosis

Reverse Osmosis (RO) System

In RO, a micro-porous (less than 10 A^0) semi-permeable membrane is used for separating dissolved salts from saline feed water. As shown in Fig. 4, the mineral ions get retained by the membrane and the water molecules are allowed to permeate through, thus achieving purification/desalination. Depending on the amount of total dissolved salts in the feed water, its osmotic pressure and thereby the operating pressure varies.

In the RO system, saline feed water is first passed through a 5 micron cut-off cartridge filter to remove suspended or colloidal particles. The filtered water is then passed through a polyamide based, spiral wound RO membrane with the help of a DC pump directly connected to the PV panels (40W) without any battery backup. The RO element is of 1.8 in. diameter & 12 in. long. Fig. 5 shows the process schematic of the RO system.

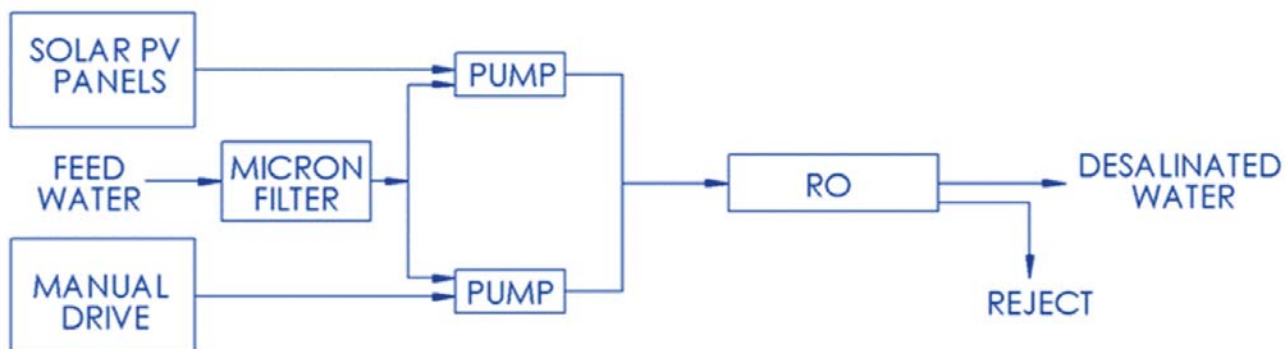**Fig. 3:   Process Schematic of the UF System**

Fig. 5:   Process Schematic of the RO System

Manual Drive

The mechanical pumps are operated by transferring the rotational movement of the hand – wheel or pedal with the help of a chain-pulley system.

Demonstration Units in BARC

The rural-friendly water treatment units developed and successfully demonstrated in BARC are shown below.

Foot/pedal operated RO/UF Units

A. Hand operated UF units (Fig. 6a & 6b)

Fig. 6: (a)   Capillary UF module (b) Multiple UF Candles

B. Foot operated RO/UF unit (Fig. 7)

Fig. 7: Foot operated RO/UF units

C. Bicycle-mounted, foot/pedal operated RO & UF units (Fig. 8). The unit being mobile, can be moved to nearby locations to treat and supply drinking water.

Fig. 8: Bicycle-mounted,   foot/pedal operated RO / UF units

Bicycle-mounted, RO / UF unit operated with hybrid power system

In order to ease the operation, hybrid energy sources (manual & electrical) are incorporated in this unit (Fig. 9). It can be operated with a mechanical pump

Fig. 9:   Bicycle-mounted, RO / UF unit operated   with hybrid power system

driven by bicycle pedalling or an electric pump driven by solar energy through PV panels. When light energy strikes the semi-conductor type solar cells, electrons are released and direct current (DC) is generated. Each pump is connected to separate UF/RO element. The modules can be operated one at a time or in parallel. If operated in parallel, the production capacity will be double. The unit has got mobility too.

Typical Performance Data of the Systems

The typical / indicative performance data of the UF & RO units are given in the Tables – 1 & 2.

Conclusion

The technical feasibility and economic viability of manually operated water treatment units for sustained production of safe drinking water in areas where scarcity of power and water co-exists have been demonstrated. These systems have the flexibility of accommodating any site-specific modifications for field deployment. Realization of deployment will be possible only by creating awareness on the importance and essentiality of safe drinking water among the people and with the cooperation of local administration, NGOs, rural ministries and the related Govt. departments.

Table 1: Typical Performance Data of the UF Units

Parameters	Candle UF	Capillary UF
Feed Flow (lit/min)	1	1.5
Product Flow (lit/min)	1	1.5
Product Turbidity (NTU)	1	1
Feed Turbidity (NTU)	50	50
Pressure (bar)	1 - 2	1 - 2

Table 2: Typical Performance Data of the RO Units

Parameters	PV based Unit	Mechanical Unit
Product Flow (lit/min)	0.15	0.15
Feed Flow (lit/min)	0.4	0.6
Feed Salinity (ppm)	1000	1000
Product Salinity (ppm)	90 -100	90 -100
Pressure (bar)	3-4	3-4
PV Power Input (W)	40	——-

References

1. "India's ground water table to dry up in 15 years", www.deccanherald.com
2. "Contaminated water kills one, sparks blame game", www.thehindu.com
3. "Downstream-processing", www.slideshare.net.

Radiation Technology for Cleaner India

Ahmedabad Municipal Corporation and Bhabha Atomic Research Centre sign MoU to set up a Sewage Sludge Hygienisation Plant at Ahmedabad.

On 21st April, 2015 India entered into a new era of utilizing advanced technology of Radiation Processing for Hygienising Sewage Sludge by signing of MoU between BARC and Ahmedabad Municipal Corporation. BARC will provide all technical and scientific support for setting up a 100 tons per day dry sewage sludge hygienisation Cobalt -60 Gamma Irradiation Plant at Ahmedabad. Large quantities of sludge is produced at various Sewage Treatment Plants and is disposed in an unorganized manner resulting in environmental pollution and spread of diseases. The sludge produced carries a heavy microbiological load and therefore its disposal has been a challenge to the urban development authorities. Bacterial counts including pathogens generally observed in sludge can vary between 10^5 to 10^9 per gram. Sludge also contains worms, ova, viruses, helminthes, weeds etc. It also contains toxic heavy metals and organic pollutants like pesticides, polyaromatic hydrocarbons, drugs and other persistent pollutants. Sludge is a rich source of many macro (Nitrogen, Phosphorous, Potassium), micro nutrients(Zinc ,Iron, Copper, Manganese)and organic carbon essential for soil. If the sludge can be treated in an effective and economic way to meet the prescribed norms, it can be recycled by using it on land for various applications including agriculture. High energy gamma radiation from Cobalt-60 can kill pathogens, reduce odours and degrade organic chemical contaminants and thus making sludge safer for use or disposal. With this initiative of Ahmedabad Municipal Corporation and BARC, a beginning has been made to utilize advanced technology for hygienising sludge for cleaner India (Swachcha and Swastha Bharat).

The MoU was signed by Smt. D. Thara, Municipal Commissioner, Ahmedabad on behalf of Ahmedabad Municipal Corporation and Dr. K.L. Ramakumar, Director, Radiochemistry and Isotope Group on behalf of Bhabha Atomic Research Centre in the presence of Dr. Lalit Varshney, Head, Radiation Technology Development Division, Dr. G. Ganesh, Head, TT&CD and other senior officials from Ahmedabad Municipal Corporation, BRIT and BARC.

From left to right:-. Shri C.R. Kharsan, Shri M. Thennarasan, Dr. Lalit Varshney, Smt. D. Thara, Dr. K.L. Ramakumar, Shri T.M. Lad, Smt. Darshana Patel and Shri Biren Raval

Super Computing Facility Building at BARC